HHS Public Access

Author manuscript

Sci Immunol. Author manuscript; available in PMC 2026 June 05.

Published in final edited form as:

Sci Immunol. 2026 February 20; 11(116): eaed7439. doi:10.1126/sciimmunol.aed7439.

RORγt⁺ Dendritic Cells Are a Distinct Lymphoid-Derived Lineage

Patrick Fernandes Rodrigues[1,*,°], **Shitong Wu**[1,°], **Tihana Trsan**[1], **Bishan Bhattarai**[1], **Santosh K. Panda**[1], **José Luís Fachi**[1], **Marina Cella**[1,2], **Marco Colonna**[1,*]

[1]Department of Pathology and Immunology, Washington University School of Medicine in Saint Louis, Saint Louis, MO, USA.

[2]Present Address: Broad Institute of MIT and Harvard, Cambridge, MA

Abstract

How tolerogenic dendritic cell (DC) lineages are established to prevent inappropriate immune responses to commensals and food antigens remains unclear. We identify RORγt$^+$ DCs as a distinct lymphoid-derived lineage to safeguard intestinal tolerance. Using lineage tracing and single-cell transcriptomics, we unveiled bone marrow–resident *Rorc(t)*$^+$ progenitors, which include a RORγt$^+$ innate lymphoid progenitor (RILP) that generates both ILC3s and RORγt$^+$ DCs, and a pre-RORγt$^+$ DC precursor committed exclusively to the RORγt$^+$ DC lineage. RORγt$^+$ DC development required the *Rorc* +7 kb enhancer, whose accessibility was regulated by the repressors REV-ERBα and REV-ERBβ, and depended on the transcription factors PRDM16 and PU.1 for lineage commitment. Loss of any of these regulators abrogated RORγt$^+$ DC differentiation, reduced peripheral T_{reg} induction, and skewed toward T helper 2 responses. Together, these findings define RORγt$^+$ DCs as a lymphoid-derived lineage whose enhancer- and transcription factor–driven development is essential for peripheral Treg-mediated immune homeostasis.

One-sentence summary:

A distinct lymphoid progenitor generates RORγt$^+$ DCs via a REV-ERB–controlled RORγt enhancer and PRDM16–PU.1-transcriptional programs

INTRODUCTION

Tolerance to harmless antigens, such as those derived from commensal microbiota or food proteins, is maintained by antigen-presenting cells (APCs), which promote regulatory immune responses by priming regulatory T (T_{reg}) cells (1–3). Recent studies have described a new family of RORγt$^+$ APCs in mice and humans, referred to as Thetis cells (TC), tolerogenic dendritic cells (tolDCs), extrathymic aire-expressing cells (eTAC), Janus cells

*Corresponding authors: mcolonna@wustl.edu and patrickr@wustl.edu.
°These authors contributed equally to this work

Author contributions:

P.F.R. and M.Co. conceived the project. P.F.R. and S.W. designed the experiments and analyzed data. P.F.R., S.W., T.T. and J.L.F. performed experiments. P.F.R performed computational analysis. B.B., S.K.P., M.Ce. provided intellectual input, protocols, and reagents. P.F.R., S.W. and M.Co. wrote the manuscript.

Competing interests: Authors declare that they have no competing interests.

or RORγt$^+$ dendritic cells (RORγt$^+$ DCs, the term used in this paper) (4–15). These cells play a pivotal role in preventing inflammatory responses to gut microbes and dietary antigens. Mice lacking RORγt$^+$ DCs fail to induce peripherally derived regulatory T (pT$_{reg}$) cells against oral antigens and instead develop increased Th2 responses and allergic inflammation. Thus, RORγt$^+$ DCs are essential for maintaining unresponsiveness to harmless microbiota and dietary antigens, thereby preserving intestinal homeostasis and preventing disorders such as food allergy and inflammatory bowel disease (8, 9, 11).

RORγt is a transcription factor best known for driving the development of lymphocyte lineages such as Th17 cells and group 3 innate lymphoid cells (ILC3s) (16–18). Consistent with this, RORγt$^+$ DCs share some phenotypic features with ILC3s. However, they also display many hallmark properties of conventional DCs, including expression of the DC lineage-specific transcription factor ZBTB46 and high levels of MHC class II (5, 8–11). Unlike RORγt$^+$ ILC3s, which are IL-7Rα$^+$ and CXCR6$^+$, RORγt$^+$ DCs do not express these markers, providing a clear way to distinguish the two cell types. Transcriptional and epigenetic profiling has further shown that RORγt$^+$ DCs cluster more closely with classical DCs than with ILC3s (5, 8–11). Functionally, RORγt$^+$ DCs reside in the small intestine, where they capture and process gut-derived antigens, then upregulate CCR7 and migrate to draining lymph nodes (8). There, they prime naïve CD4$^+$ T cells and skew differentiation toward Foxp3$^+$ RORγt$^+$ pT$_{reg}$ rather than effector subsets (2, 5, 6, 8, 9, 11). Altogether, RORγt$^+$ DCs combine limited ILC3-like features with the molecular and functional toolkit of classical DCs, behaving as professional antigen-presenting cells specialized for tolerance. This dual identity raises a fundamental question: do RORγt$^+$ DCs share the lymphoid origin of ILC3s, the myeloid origin of most DCs, or do they represent a distinct lineage of tolerogenic DCs?

Classical DCs are largely derived from bone marrow–resident myeloid progenitors, including the monocyte–dendritic cell progenitor (MDP) (19, 20) and the common DC progenitor (CDP) (21–23). However, accumulating evidence indicates that subsets of DCs can also arise from distinct non-myeloid progenitors, including lymphoid-derived precursors (24–31). In line with this, in vitro studies and lineage tracing experiments with hCD2 lineage tracer mice have suggested that RORγt$^+$ DCs develop through a lymphoid-biased pathway (11, 12). Most evidence supporting a lymphoid origin comes from mouse neonates, when a wave of RORγt$^+$ DCs colonizes gut-associated lymphoid tissues in parallel with microbiota establishment (5, 11, 32). Whether adult RORγt$^+$ DCs are sustained by the same lymphoid progenitor pool, or whether they can also emerge from myeloid progenitors later in life, has not been resolved. Moreover, the precise upstream progenitor that gives rise to RORγt$^+$ DCs and how its fate is directed away from other lineages, including ILC3s (27), remain undefined.

ILC3 and RORγt$^+$ DC development is under strict transcriptional control. A cis-regulatory enhancer located +7 kb downstream of the *Rorc* promoter (+7kbE) is indispensable for maintaining this subset, and the transcriptional coregulator PRDM16 is crucial for RORγt$^+$ DCs: in its absence, RORγt$^+$ DCs fail to develop and do not induce pT$_{reg}$ responses to food antigens which leads to loss of tolerance (8, 11). Yet, the regulatory mechanisms that establish and maintain these transcriptional programs remain largely unknown.

In this study, we identify RORγt$^+$ DCs as a lymphoid-derived antigen-presenting cell lineage that develops efficiently in both neonates and adults, arising predominantly from IL-7R-expressing lymphoid progenitors. Single-cell and functional analyses identify a RORγt$^+$ innate lymphoid progenitor (RILP) that generates both MHC-II$^+$ ILC3s and RORγt$^+$ DCs, and a pre-RORγt$^+$ DC precursor committed exclusively to the RORγt$^+$ DC lineage. RORγt$^+$ DC development requires the Rorc +7 kb enhancer and is governed by a transcriptional network in which REV-ERBα and REV-ERBβ maintain enhancer accessibility, while PRDM16 and PU.1 act downstream to stabilize lineage commitment, particularly of RORγt$^+$ DC II–IV subsets. Together, these findings establish a developmental and transcriptional program that defines RORγt$^+$ DC specification as a distinct lymphoid pathway within the DC lineage.

RESULTS

RORγt$^+$ DCs are of lymphoid origin independent of mouse age

We previously showed that RORγt$^+$ DCs originate from lymphoid-derived progenitors in 15-day-old pups in vitro (11). However, it remained unclear whether RORγt$^+$ DCs in adult mice also arise from lymphoid progenitors or from distinct precursors. To address this question, we compared the output of total bone marrow (BM) cells from 15-day-old pups and adult *Gm38411*$^{iCre\text{-}hCD2}$ Rosa26^{tdTomato} mice cultured under conditions that promote RORγt$^+$ DC development (FLT3L, IL-7, SCF), which have been previously validated to support differentiation of RORγt$^+$ DCs in vitro (11). In these mice, hCD2 and Cre expression are driven by *Gm38411*, an antisense long-noncoding RNA that shares the promoter region with RORγt and precisely mirrors RORγt expression (11). Thus, the system serves both as a direct reporter of *Gm38411*/RORγt activity (via hCD2 expression) and as a lineage-tracing tool marking cells that have expressed *Gm38411*/RORγt (via tdTomato expression) (11). When BM cells from 15-day-old pups or adult mice were cultured under conditions that promote RORγt$^+$ DC development, both groups generated comparable numbers of RORγt$^+$ DCs (Fig. 1, A and B). In contrast, type 1 (DC1) and type 2 (DC2) DC outputs were higher in adult cultures, likely reflecting enhanced myelopoiesis in adults that supports greater overall DC yields (32).

To determine whether RORγt$^+$ DCs in adult mice are derived from lymphoid or myeloid BM progenitors, we sort-purified three BM populations: IL-7R$^+$ lymphoid progenitors (IL-7R$^+$ LP), IL-7R$^-$ M-CSFR$^-$ double-negative DC progenitors (DN DCP), which represent a mixed lymphoid–myeloid precursor pool (25, 28, 33), and myeloid CD115$^+$ CDPs. Each population was cultured with FLT3L, IL-7, and SCF for four days, a time point at which their developmental output peaks. As a positive control, we also included lymphoid-primed multipotent progenitors (LMPP), which retain lymphoid and some myeloid potential. In adult mice, RORγt$^+$ DCs were generated most efficiently from IL-7R$^+$ LP, whereas LMPP and DN DCP showed only limited potential, and CDPs produced almost no RORγt$^+$ DCs (Fig. 1, C and D and fig. S1A). These results demonstrate that RORγt$^+$ DC development occurs in both pups and adults, and in both cases relies primarily on IL-7R$^+$ LP.

Single-cell profiling of in vitro-generated RORγt$^+$ DCs

To validate the identity of in vitro generated RORγt$^+$ DCs, we performed scRNA-seq on CD3$^-$ B220$^-$ Ly6C$^-$ hCD2$^+$ tdTomato$^+$ cells from cultured BM of 15-day old *Gm38411*$^{iCre\text{-}hCD2}$ R26^{tdTomato} mice. After quality control, we projected 23,360 cells onto a Uniform Manifold Approximation and Projection (UMAP) (Fig. 1E). Three clusters were defined based on marker gene expression and differentially expressed genes (DEGs) filtering for DNA-binding or cell surface proteins (Fig. 1, F and G and data file S1, A to C). All clusters expressed core RORγt$^+$ DC/ILC3 genes, including *Rorc*, *Gm38411*, *Lingo4*, *Nrp1*, *Ptprc*, *Ltb*, and *Il1r1* (fig. S1B). Clusters 0 and 2 corresponded to ILC3s, marked by *Rora*, *Maf*, *Tcf7*, *Il23r*, and *Cxcr6*. Cluster 2 additionally expressed proliferation-associated genes (*Mki67*, *Kif4*, *Smc2*, *Ezh2*). In contrast, Cluster 1 expressed RORγt$^+$ DC-associated genes, including *Spi1*, *Prdm16*, *Runx3*, *H2-Ab1*, *Itgam*, and *Itgax* (Fig. 1, F and G and data file S1). Overall, our scRNA-seq analysis shows that culturing total BM cells under RORγt$^+$ DC promoting conditions yields hCD2$^+$ tdTomato$^+$ cells that include both RORγt$^+$ DCs and ILC3s.

Lymphoid precursors develop into RORγt$^+$ DCs in vivo

We next investigated whether IL-7R$^+$ LP, which readily generate RORγt$^+$ DCs in vitro, can also give rise to this lineage in vivo, where developmental cues and microenvironmental signals are more complex. At the same time, we asked whether CDPs, which represent a canonical myeloid pathway of DC development, contribute to the RORγt$^+$ DC compartment under physiological conditions. We sort-purified LMPP, IL-7R$^+$ LP, DN DCP, and CDPs from *Gm38411*$^{iCre\text{-}hCD2}$ R26^{tdTomato} 15-day-old pups or adults and transferred them into sub-lethally irradiated congenic recipients (Fig. 1, H to K). Seven days later, we assessed donor-derived RORγt$^+$ DCs in the spleen. LMPP, IL-7R$^+$ LP, and DN DCP from both pups (Fig. 1, H and I and fig. S1C) and adults (Fig. 1, J and K and fig. S1D) generated RORγt$^+$ DCs, whereas CDPs had negligible potential regardless of age (Fig. 1, H to K and fig. S1C and D). Therefore, lymphoid-primed progenitors, particularly IL-7R$^+$ LP, are the main source of RORγt$^+$ DCs in vitro and in vivo, independent of donor age, while myeloid CDPs lack this capacity. These findings place RORγt$^+$ DCs within the lymphoid branch of DC development.

RORγt$^+$ DCs are broadly present in lymphoid tissues

RORγt$^+$ DCs induce pT$_{reg}$ in the mesenteric lymph nodes (mLN) (5, 6, 8, 9, 11). To determine whether RORγt$^+$ DCs are present in lymphoid tissues beyond the mLNs and whether they display phenotypic heterogeneity across sites, we analyzed multiple lymphoid compartments from *Gm38411*$^{iCre\text{-}hCD2}$ R26^{tdTomato} mice by flow cytometry, including BM, spleen, and lymph nodes draining the skin (sLN), cervical regions (cLN), and intestine (mLN). In the BM, we detected a small population of Lin$^-$ CD3$^-$ CD16/32$^-$ hCD2$^+$ tdTomato$^+$ cells. In peripheral lymphoid tissues, we identified CXCR6$^-$ CD127$^-$ tdTomato$^+$ hCD2$^+$ RORγt$^+$ DCs across all LNs and the spleen, with the spleen harboring the largest total number of RORγt$^+$ DCs (fig. S2, A to F).

To map RORγt$^+$ DCs across tissues with higher resolution, we performed scRNA-seq on sorted CD3$^-$ tdTomato$^+$ hCD2$^-$ and hCD2$^+$ cells isolated from BM, spleen, sLNs, cLNs,

and mLNs of 15-day-old pups and adult *Gm38411*$^{iCre\text{-}hCD2}$ R26^{tdTomato} mice, using sample hashtagging to track age and tissue of origin. After quality control, 16,250 cells were analyzed, resulting in five clusters. Clusters 0 and 1 corresponded to ILC3s, expressing *Il7r*, *Cxcr6, Rora*, *Il23r*, *Klf4*, and *Runx1*. Clusters 2 and 3 represented RORγt$^+$ DCs which expressed *Prdm16*, *Runx3*, *Itgax*, *Pigr*, and *Ccr7*. Cluster 4 expressed proliferation, DNA replication, and mitotic genes (*Mki67*, *Pclaf*, *Ccna2*, *Mcm2*, *Lig1*, *Rrm2*, *Rad51b*, *Kif11*, *Kif15*, *Cenpf*, *Cenpe*, *Birc5*) and was annotated as a proliferative Mki67$^+$ cluster (Fig. 2A and data file S2A).

TC and RORγt$^+$ DCs have been divided into four transcriptionally distinct subsets (here called RORγt$^+$ DC I–IV) (5, 11). To investigate whether their distribution varies by tissue and further identify potential progenitors, we reclustered RORγt$^+$ DC clusters 2 and 3 together with proliferative cluster 4. Reclustering yielded 3381 cells distributed into six clusters (Fig. 2B). Clusters 0, 1, 2, 3, and 5 were represented across all peripheral lymphoid organs, whereas cluster 4 derived exclusively from BM. Cluster 5 also contained ~25% BM-derived cells (Fig. 2C). Differential expression analysis focusing on cell surface receptors (Fig. 2D and data file S2B) and DNA-binding proteins (Fig. 2E and data file S2C) revealed that Cluster 0 corresponded to RORγt$^+$ DC II (*Itgax*, *Epcam*, *Prdm16*, *Spi1*, *Ly75*, *Tlr12*, *Runx3*), while Cluster 1 matched RORγt$^+$ DC I (*Aire*, *Cd200*, *Nrxn1*, *Ebf1*, *Meis1*) (Fig. 2, D to F and data file S2, B and C). Cluster 3 expressed *Ccr7*, *Itgb1*, *Itgam*, *Etv3*, *Spic*, *Spib*, and *Elf4*, consistent with RORγt$^+$ DC III–IV. Cluster 2 was annotated as ILC3s (*Il7r*, *Cxcr6*, *Cd226*, *Rora*, *Maf*). Pearson correlation analysis comparing Clusters 0, 1, and 3 to our previously published scRNA-seq dataset (11), together with integrative overlap of all clusters across our dataset and three recently published scRNA-seq datasets (8, 9, 11), confirmed these annotations (fig. S2, G and H). Notably, Cluster 4, which derived almost exclusively from BM, expressed *Rorc* alongside genes characteristic of BM progenitors, including *Flt3*, *Lifr*, *Cd93*, *Cd48*, *Id2*, *Ikzf1*, and *Bcl11a*. This cluster was therefore annotated as *Rorc*$^+$ BM cells (Fig. 2, C to F and data file S2, B and C).

Rorc$^+$ BM cells branch into RORγt$^+$ DC and ILC3 lineages

Given that *Rorc*$^+$ BM cells were transcriptionally distinct from ILC3s and RORγt$^+$ DCs from peripheral tissues in the UMAP distribution, we analyzed them in greater detail. We reclustered the *Rorc*$^+$ BM population and identified two distinct subsets: *Rorc*$^+$ BM cells 1 (Cluster 0) and *Rorc*$^+$ BM cells 2 (Cluster 1) (Fig. 2G). Differential expression analysis showed that *Rorc*$^+$ BM cells 1 displayed a transcriptional profile reminiscent of innate lymphoid precursors (*Il7r*, *Tcf7, Cd37*, *Cd244a*, *Rora*, *Nfil3*, *Tox* and *Maf*), while *Rorc*$^+$ BM cells 2 more closely resembled RORγt$^+$ DCs (*Itgax*, *Prdm16*, *Spi1*, *Irf8*, *Nr1d1*, *Tlr12*, *Clec10a*, *Ly75*, *Mgl2*, and *Cd101*) (Fig. 2, H to J and fig. S2, I and J and data file S3). This suggests that *Rorc*$^+$ BM cells comprise two precursor subsets, RORγt$^+$ innate lymphoid progenitors (RILP) and pre-RORγt$^+$ DCs.

We further validated the existence of these subsets by flow cytometry in *Gm38411*$^{iCre\text{-}hCD2}$ R26^{tdTomato} adult mice. Using CD127 and CD11c expression within Lin$^-$ CD3$^-$ CD16/32$^-$ B220$^-$ tdTomato$^+$ hCD2$^+$ *Rorc*$^+$ BM cells, we identified tdTomato$^+$ hCD2$^+$ CD127$^{+/-}$ CD11c$^-$ *Rorc*$^+$ BM cells 1 (RILP) and tdTomato$^+$ hCD2$^+$ CD127$^-$ CD11c$^+$

Rorc^{+} BM cells 2 (pre-RORγt^{+} DCs) (Fig. 3A). To assess their developmental potential, we sort-purified Lin^{-} CD3^{-} CD16/32^{-} B220^{-} tdTomato^{+} hCD2^{+} *Rorc*$^{+}$ BM cells from adult *Gm38411*$^{iCre\text{-}hCD2}$ R26^{tdTomato} mice and cultured them for 3 days under RORγt^{+} DC–promoting conditions. After 3 days, both hCD2^{+} tdTomato^{+} CD11c^{-} MHC-II^{+} ILC3s and hCD2^{+} tdTomato^{+} CD11c^{+} MHC-II^{+} RORγt^{+} DCs were detected (Fig. 3, B and C).

Due to the low abundance of RILP and pre-RORγt^{+} DCs in the BM, we established an in vivo system to expand these progenitor subsets. *Gm38411*$^{iCre\text{-}hCD2}$ R26^{tdTomato} mice were injected with a mixture of SCF, Flt3L and IL-7 (Fig. 3, D to G and fig. S3, A and B). Seven days after the first injection, we observed an increase in *Rorc*$^{+}$ BM cells, including pre-RORγt^{+} DCs and RILP, as well as mature RORγt^{+} DCs I–IV and ILC3s in the spleen and mLNs (Fig. 3, D to G and fig. S3, A and B). To assess developmental potential, both expanded progenitor subsets were cultured for three days under RORγt^{+} DC–promoting conditions. RILP generated both tdTomato^{+} hCD2^{+} CD11c^{-} MHC-II^{+} ILC3s and tdTomato^{+} hCD2^{+} CD11c^{+} MHC-II^{+} RORγt^{+} DCs, whereas pre-RORγt^{+} DCs differentiated predominantly into RORγt^{+} DCs (Fig. 3, H to K). We also evaluated the in vivo potential of *Rorc*$^{+}$ BM cells by transferring expanded Lin^{-} tdTomato^{+} hCD2^{+} *Rorc*$^{+}$ BM cells from *Gm38411*$^{iCre\text{-}hCD2}$ R26^{tdTomato} mice into sub-lethally irradiated congenic recipients. Three days after transfer, both tdTomato^{+} hCD2^{+} CD127^{+} CD11c^{-} MHC-II^{+} ILC3s and tdTomato^{+} hCD2^{+} CD127^{-} CD11c^{+} MHC-II^{+} RORγt^{+} DCs were detected in the spleen (Fig. 3, L and M). Together, these findings demonstrate that *Rorc*$^{+}$ BM cells comprise two transcriptionally distinct precursors. RILP have the potential to generate MHC-II+ ILC3s and RORγt^{+} DCs, while pre-RORγt^{+} DCs generate RORγt^{+} DCs only.

RORγt^{+} DC development is impaired in Rag2$^{-/-}$γc$^{-/-}$ mice

To further confirm the lymphoid origin of RORγt^{+} DCs, we analyzed hCD2^{Cre} R26^{tdTomato} mice, which lineage trace cells of lymphoid origin (34). The majority of RILP and pre-RORγt^{+} DCs in the BM, as well as mature splenic ILC3s, RORγt^{+} DC I and RORγt^{+} DC II–IV, were lineage traced in hCD2^{Cre} R26^{tdTomato} mice (Fig. 3N). To assess whether RORγt^{+} DCs can be reliably detected in non-reporter mice, we performed intracellular RORγt staining in *Gm38411*$^{iCre\text{-}hCD2}$ mice. Intracellular RORγt staining overlapped with hCD2^{+} *Rorc*$^{+}$ BM cells, including RILP and pre-RORγt^{+} DCs, as well as mature RORγt^{+} DC I, RORγt^{+} DC II–IV, and ILC3s (fig. S3, C to F). In addition, *Rorc(t)*$^{GFP/GFP}$ mice, which lack functional RORγt expression, were devoid of RORγt^{+} cells, excluding background staining by RORγt antibodies (fig. S3, G and H). After these validation experiments, we examined RORγt^{+} DC development in *Rag2*$^{-/-}$*γc*$^{-/-}$ mice. While RILP and pre-RORγt^{+} DCs in the bone marrow were not affected, mature splenic CD200^{+} RORγt^{+} DC I and EPCAM^{+} RORγt^{+} DC II–IV were strongly reduced (Fig. 3, O to R and fig. S3I). Consistent with the known phenotype of *Rag2*$^{-/-}$*γc*$^{-/-}$ mice, NK cells, B cells, and T cells were absent. We also observed a marked reduction in pDCs and DC2s, whereas granulocytes were unaffected (fig. S3I). Together, these data indicate that RORγt^{+} DCs arise from lymphoid progenitors traced by hCD2^{Cre} R26^{tdTomato} and require cytokine signaling through the common γ-chain.

The Rorc +7kb enhancer is essential for RORγt$^+$ DC development

A cis-regulatory enhancer element located +7 kb downstream of the *Rorc* gene transcriptional start site (*Rorc* +7kbE) was recently shown to be crucial for maintaining tolerance to food antigens by regulating the presence and function of RORγt$^+$ DCs (8, 11). Mice lacking this element, hereafter referred to as Rorc$_E$+7kb$^{Δ/Δ}$, lose the ability to prime pT$_{reg}$ and instead mount an enhanced Th2 response (8, 11). However, it remains unclear whether the phenotype in Rorc$_E$+7kb$^{Δ/Δ}$ mice is due to impaired development of RORγt$^+$ DCs from BM progenitors or defective function of RORγt$^+$ DCs. To address whether the *Rorc* +7kbE is required for RORγt$^+$ DC development, we evaluated whether *Rorc*$^+$ BM cells, including pre-RORγt$^+$ DCs, are affected in Rorc$_E$+7kb$^{Δ/Δ}$ mice (Fig. 4A). We observed an overall reduction of both RILP and pre-RORγt$^+$ DCs in Rorc$_E$+7kb$^{Δ/Δ}$ mice compared with Rorc$_E$+7kb$^{WT/WT}$ controls. This reduction was consistent regardless of whether pre-RORγt$^+$ DCs were identified using CD11c (Fig. 4A, left) or PRDM16 (Fig. 4A, right) staining, indicating that the *Rorc* +7kbE is required for RORγt$^+$ DC development.

To confirm a developmental defect, we cultured total BM cells from adult Rorc$_E$+7kb$^{WT/WT}$ and Rorc$_E$+7kb$^{Δ/Δ}$ mice under RORγt$^+$ DC–promoting conditions. After 8 days, we observed a reduction in both MHC-II$^+$ RORγt$^+$ CXCR6$^+$ ILC3s and MHC-II$^+$ RORγt$^+$ CXCR6$^-$ CD11c$^+$ PRDM16$^+$ RORγt$^+$ DCs in the absence of the *Rorc* +7kbE (Fig. 4, B and C). To validate these findings in vivo, we performed competitive differentiation assays by transferring sort-purified LMPP, IL-7R$^+$ LP, DN DCP, or CDP from Rorc$_E$+7kb$^{Δ/Δ}$ and congenically marked Rorc$_E$+7kb$^{WT/WT}$ mice into sub-lethally irradiated CD45.1$^+$ recipients. Seven days later, Rorc$_E$+7kb$^{Δ/Δ}$ progenitors showed a markedly reduced capacity to generate both RORγt$^+$ DCs and ILC3s, irrespective of progenitor type. In contrast, development of conventional DC1 and DC2 was unaffected when Rorc$_E$+7kb$^{Δ/Δ}$ precursors competed with WT counterparts (Fig. 4, D and E and fig. S4, A to C). Importantly, even in the absence of the *Rorc* +7kbE, LMPP, IL-7R$^+$ LP, and DN DCP retained the highest relative potential to give rise to RORγt$^+$ DCs and ILC3s, whereas CDP contributed minimally to these lineages and instead generated DC1 and DC2 (Fig. 4, D to F and fig. S4, A to C). We also assessed whether other DCs are affected in Rorc$_E$+7kb$^{Δ/Δ}$ mice, but neither pDCs nor pDC-like cells or DC2 subsets were altered (fig. S4, D and E). Thus, both RORγt$^+$ DCs and ILC3s arise from lymphoid progenitors, but their developmental potential depends on the *Rorc* +7kbE, which is dispensable for the generation of conventional DC subsets.

RORγt$^+$ DC development requires REV-ERBα and REV-ERBβ

The mechanisms regulating the *Rorc* +7kbE and enabling it to drive the development of RORγt$^+$ DCs remain unknown. The circadian transcriptional repressors REV-ERBα and REV-ERBβ are known to suppress NFIL3, itself a repressor of RORγt (35). We previously showed that deletion of *Nr1d1* (encoding REV-ERBα) and *Nr1d2* (encoding REV-ERBβ) results in reduced RORγt expression due to NFIL3 upregulation, which acts through a cis-regulatory element within the *Rorc* locus (36–38). Consistent with this, ILC3s isolated from *Vav*^{iCre} *Nr1d1*/*Nr1d2*$^{fl/fl}$ mice exhibited reduced chromatin accessibility at the *Rorc* +7kbE (Fig. 5A) (38). Notably, *Nr1d1* was among the differentially expressed genes in pre-RORγt$^+$ DCs (Fig. 2, H and J), pointing to a potential regulatory role. Based on this, we hypothesized that REV-ERBα and REV-ERBβ are critical for RORγt$^+$ DC development.

We analyzed RORγt$^+$ DC and ILC3 frequencies in the spleen (Fig. 5, B and C) and mLN (Fig. 5, D and E and fig. S5A) of *Vav*^{iCre} *Nr1d1*/*Nr1d2*$^{fl/fl}$ mice. In the spleen, the number of B220$^-$ CD3$^-$ Ly6C$^-$ RORγt$^+$ MHC-II$^+$ CXCR6$^-$ PRDM16$^+$ DCs was reduced compared to control *Nr1d1*/*Nr1d2*$^{fl/fl}$ mice, whereas B220$^-$ CD3$^-$ Ly6C$^-$ RORγt$^+$ MHC-II$^+$ PRDM16$^-$ CXCR6$^+$ Lti-like ILC3s were modestly increased (Fig. 5, B and C). Similarly, in the mLN we observed a reduction in RORγt$^+$ DCs, while the frequency of MHC-II$^+$ ILC3s remained unchanged (Fig. 5, D and E and fig. S5A). Because loss of RORγt$^+$ DCs in Rorc$_E$+7kb$^{\Delta/\Delta}$ mice was previously shown to impair pT$_{reg}$ induction and enhance Th2 responses (8, 11), we asked whether *Nr1d1*/*Nr1d2* deficiency produced a similar phenotype. Indeed, *Vav*^{iCre} *Nr1d1*/*Nr1d2*$^{fl/fl}$ mice displayed reduced pT$_{reg}$ frequencies and numbers, accompanied by expansion of Th2 cells in the mLN, while Th17 cells were unaffected (Fig. 5, F and G and fig. S5B).

To further assess the impact of REV-ERBα and REV-ERBβ on RORγt$^+$ DC development, we cultured BM cells from *Nr1d1*/*Nr1d2*$^{fl/fl}$ and *Vav*^{iCre} *Nr1d1*/*Nr1d2*$^{fl/fl}$ mice under RORγt$^+$ DC-promoting conditions. After 8 days, cultures from *Vav*^{iCre} *Nr1d1*/*Nr1d2*$^{fl/fl}$ mice showed a reduction in RORγt$^+$ MHC-II$^+$ CD127$^-$ CXCR6$^-$ CD11c$^+$ PRDM16$^+$ RORγt$^+$ DCs as well as RORγt$^+$ MHC-II$^+$ CD127$^+$ CXCR6$^+$ ILC3s, whereas DC1 and DC2 outputs were unchanged (Fig. 5, H and I and fig. S5C). No changes were observed within the splenic DC compartment in *Vav*^{iCre} *Nr1d1*/*Nr1d2*$^{fl/fl}$ mice (fig. S5D). Overall, these findings indicate that REV-ERBα and REV-ERBβ regulate the development of RORγt$^+$ DCs and ILC3s by controlling accessibility at the *Rorc* +7kbE, thereby linking transcriptional regulators to lineage specification of RORγt$^+$ immune subsets.

PRDM16 is required for RORγt$^+$ DC development

PRDM16 is a transcriptional coregulator known for controlling cell fate decisions in multiple tissues, including hematopoietic and stromal lineages (39–44). PRDM16 is highly expressed in RORγt$^+$ DCs (5, 10–12) and its deletion in tolDCs was recently shown to disrupt pT$_{reg}$ induction to harmless antigens, resulting in aberrant Th2 responses and impaired intestinal tolerance (8). Whether PRDM16 regulates RORγt$^+$ DC development or function remains unclear. To address this, we crossed *Gm38411*$^{iCre\text{-}hCD2}$ mice with *Prdm16*$^{fl/fl}$ mice, generating *Gm38411*$^{iCre\text{-}hCD2}$ *Prdm16*$^{fl/fl}$ mice. We first examined whether *Prdm16* deficiency affected pre-RORγt$^+$ DCs in the BM. Indeed, *Gm38411*$^{iCre\text{-}hCD2}$ *Prdm16*$^{fl/fl}$ mice displayed a reduction in pre-RORγt$^+$ DCs compared to *Prdm16*$^{fl/fl}$ controls, independent of whether gating was based on CD11c$^+$ or PRDM16$^+$ RORγt$^+$ DCs (Fig. 6, A and B and fig. S6A). By contrast, RILP frequencies were unchanged (Fig. 6, A and B). Furthermore, no differences were observed among other progenitors, including LMPP, IL-7R$^+$ LP, DN DCP, or CDP (fig. S6B). We next assessed mature RORγt$^+$ DC abundance in the mLN (Fig. 6, C and D and fig. S6C) and spleen (fig. S6, D and E). In both tissues, deletion of *Prdm16* led to reduced numbers of Epcam$^+$ RORγt$^+$ DC II–IV subsets. However, CD200$^+$ RORγt$^+$ DC I cells were expanded (Fig. 6, C and D and fig. S6, D and E). ILC3s, DC1 and DC2 populations, as well as PRDM16 expressing splenic γδ T cells, remained unaffected (fig. S6, C to E).

Because PRDM16$^+$ RORγt$^+$ DCs have been shown to mediate the induction of pT$_{reg}$ cells against commensals and food antigens, we next analyzed T cell subsets in the mLN of *Prdm16*$^{fl/fl}$ and *Gm38411*$^{iCre\text{-}hCD2}$ *Prdm16*$^{fl/fl}$ mice (Fig. 6, E and F and fig. S6, F and G). Frequencies of RORγt$^+$ FoxP3$^+$ pT$_{reg}$ were reduced, accompanied by an expansion of RORγt$^-$ FoxP3$^-$ T-bet$^-$ GATA3$^+$ Th2 cells (Fig. 6, E and F). No changes were observed in other CD4$^+$ T cell subsets, including RORγt$^-$ FoxP3$^+$ T$_{reg}$, RORγt$^+$ FoxP3$^-$ Th17, or RORγt$^-$ FoxP3$^-$ T-bet$^+$ Th1 cells (Fig. 6E and fig. S6, F and G). We also observed a reduction of pT$_{reg}$ and an increase of Th2 in the lamina propria of the small intestine, confirming the data obtained from the mLN (fig. S6, H and I). Together, these findings identify PRDM16 as a critical regulator of pre-RORγt$^+$ DC development. Notably, RORγt$^+$ DC I expand in the absence of PRDM16. However, this expansion alone is insufficient to sustain immune tolerance and restrict Th2 responses.

PU.1 is required for RORγt$^+$ DC development

PU.1, encoded by *Spi1*, is a central, dosage-dependent transcription factor that regulates hematopoiesis, with requirements that vary by lineage and developmental stage. High PU.1 levels favor myeloid differentiation, whereas lower levels bias lymphoid fate decisions (45). In lymphopoiesis, PU.1 is required for efficient LMPP formation and for normal T and B cell development, and its near-complete loss ablates most conventional lymphocytes (46, 47). In DC development, PU.1 is indispensable, as it promotes Flt3 expression, primes DC progenitors, and activates IRF8-dependent transcriptional programs required for cDC1 and cDC2 differentiation (48–50). *Spi1* is expressed in pre-RORγt$^+$ DCs as well as in mature RORγt$^+$ DC II (Fig. 2, E, H and J and data file S2C), but its role in RORγt$^+$ DC development has not been characterized. To address this, we crossed *Rorc(t)*^{Cre} mice with *Spi1*$^{fl/fl}$ mice, generating *Rorc(t)*^{Cre} *Spi1*$^{fl/fl}$ animals. We first examined whether *Spi1* deficiency affected pre-RORγt$^+$ DCs in the BM. *Rorc(t)*^{Cre} *Spi1*$^{fl/fl}$ mice displayed a substantial reduction in CD11c$^+$ and PRDM16$^+$ pre-RORγt$^+$ DCs compared with *Spi1*$^{fl/fl}$ controls (Fig. 6, G and H and fig. S7A), whereas RILP frequencies were unchanged (Fig. 6, G and H). We next assessed mature RORγt$^+$ DCs in mLN and spleen. In both tissues, *Spi1* deletion resulted in a marked reduction of EPCAM$^+$ RORγt$^+$ DC II–IV subsets, while CD200$^+$ RORγt$^+$ DC I cells were unaffected (Fig. 6, I and J and fig. S7, B to D). ILC3s, DC1, and DC2 populations were unchanged (fig. S7, B to D). In line with the observed phenotype in PU.1-deficient mice, total BM cultures from *Rorc(t)*^{Cre} *Spi1*$^{fl/fl}$ mice exhibited a defect in RORγt$^+$ DC generation, whereas ILC3 development was unaffected (fig. S7, E and F), indicating an essential role for PU.1 in RORγt$^+$ DC development.

We then analyzed CD4 T cell responses in the mLN. Frequencies of RORγt$^+$ FoxP3$^+$ pT$_{reg}$ were reduced in *Rorc(t)*^{Cre} *Spi1*$^{fl/fl}$ mice, accompanied by an increase in RORγt$^-$ FoxP3$^-$ T-bet$^-$ GATA3$^+$ Th2 cells (Fig. 6, K and L). No differences were observed in other CD4$^+$ T cell subsets, including RORγt$^-$ FoxP3$^+$ T$_{reg}$, RORγt$^+$ FoxP3$^-$ Th17 cells, or RORγt$^-$ FoxP3$^-$ T-bet$^+$ Th1 cells (Fig. 6K and fig. S7, G and H). Overall, these findings demonstrate that PU.1 is required for the development of RORγt$^+$ DC II–IV, and that loss of these cells in *Spi1*-deficiency leads to impaired pT$_{reg}$ induction and skewing toward Th2 responses.

DISCUSSION

Our study identifies RORγt$^+$ DCs as a distinct tolerogenic lineage within the antigen-presenting cell network in both neonates and adults. Unlike conventional DC1 and most DC2, which primarily arise from myeloid progenitors, are lineage traced in *Clec9a*^{Cre} mouse models, and specialize in effector T cell priming, RORγt$^+$ DCs derive from lymphoid progenitors and are uniquely dedicated to the induction of pT$_{reg}$ (5, 6, 8, 9, 11, 12, 32, 51). This dual organization of antigen-presenting cells suggests a division of labor in which one branch drives immunity while the other enforces tolerance. The lymphoid origin of RORγt$^+$ DCs is consistent with previous lineage tracing combined with single-cell transcriptomics data (11, 12, 28). Furthermore, we identify two RORγt$^+$ BM precursors: RILP, which gives rise to both MHC-II+ ILC3s and RORγt$^+$ DCs, and pre-RORγt$^+$ DCs, which are exclusively committed to the RORγt$^+$ DC lineage. This developmental hierarchy not only clarifies how RORγt$^+$ DCs emerge but also situates them developmentally closer to innate lymphoid cells than to classical DCs. Thus, RORγt$^+$ DCs are not merely a variant of conventional DCs but represent a distinct lineage specialized to maintain homeostasis.

Our results also delineate the molecular circuitry that specifies RORγt$^+$ DC lineage commitment. We demonstrate that the *Rorc* +7kbE is essential for their generation, and the circadian repressors REV-ERBα and REV-ERBβ maintain the accessibility of this regulatory element. In turn, the transcriptional coregulators PRDM16 and PU.1 are required for lineage commitment. Disruption of any of these factors abolishes RORγt$^+$ DC development, reduces pT$_{reg}$ induction, and skews responses toward Th2 immunity. Notably, our findings reveal that only RORγt$^+$ DC II–IV require PRDM16 and PU.1 for their development, whereas RORγt$^+$ DC I either expand or remain unchanged in the absence of these transcription factors. Yet, the presence of RORγt$^+$ DC I is not sufficient to induce pT$_{reg}$. We conclude that RORγt$^+$ DC I and DC II–IV arise through distinct developmental pathways and perform non-overlapping functions.

Within this emerging framework, REV-ERBα and REV-ERBβ appear to occupy an upstream position in the hierarchy controlling RORγt$^+$ DC II-IV differentiation. These factors integrate environmental, circadian, and metabolic cues to establish a permissive chromatin landscape at the +7kbE of the *Rorc* locus, thereby enabling RORγt expression. In contrast, PRDM16- and PU.1 appear to function at later checkpoints. Since RORγt-driven deletion of either factor eliminates pre-RORγt$^+$ DCs and mature RORγt$^+$ DC II–IV, PRDM16 and PU.1 specify the RORγt$^+$ DC II–IV program rather than initiate *Rorc* expression. The precise modes of interaction among these regulators remain to be fully elucidated, but their integration into a single developmental cascade provides an initial basis for understanding how development of RORγt$^+$ DC II–IV is regulated.

Beyond defining this hierarchy, our data suggest that REV-ERB–dependent control of enhancer accessibility may represent a key point of environmental regulation. REV-ERBα and REV-ERBβ are known to respond to external cues, including circadian entrainment signals (light–dark cycles, temperature rhythms), metabolic and feeding states, heme availability and cellular redox balance (52), raising the possibility that fluctuations in these

signals influence RORγt$^+$ DC abundance and function. Such regulation would provide a direct link between physiological rhythms and immune homeostasis at barrier tissues.

The mechanisms regulating RORγt$^+$ DC I specification remain largely unexplored. The prominent expression of Aire, together with *Tnfrsf11a* (RANK), a receptor that induces Aire expression in medullary thymic epithelial cells (53–56), raises the possibility that RORγt$^+$ DC I identity may be shaped by extrinsic signaling pathways. Whether RANK-mediated signals are required to establish or maintain the RORγt$^+$ DC I fate, and how such pathways relate to the apparent independence from PRDM16 and PU.1, remains an important question for future studies. Overall, this study defines a developmental pathway that sculpts tolerogenic antigen-presenting cells, and identifies potential targets for therapeutic intervention, including pharmacologic activation of REV-ERB signaling, that could be leveraged to restore tolerance in inflammatory and allergic diseases such as food allergy, asthma, and inflammatory bowel disease.

MATERIALS AND METHODS

Study design

The goal of this study was to define the developmental origin, progenitor hierarchy, and transcriptional regulation of RORγt$^+$ DCs. To address this, we used complementary in vitro and in vivo approaches in mice, including bone marrow differentiation assays, adoptive transfer experiments, lineage tracing, flow cytometry, and single-cell RNA sequencing, together with genetic loss-of-function models to assess transcriptional requirements for RORγt$^+$ DC development. Sample sizes were based on prior experience and reproducibility, with key findings confirmed in two to three independent experiments using multiple biological replicates. Animals were assigned to experimental groups based on genotype and availability, and data were analyzed using predefined gating strategies. All samples meeting predefined quality criteria were included, and data were excluded only in cases of clear technical failure.

Animals

All animals were bred and maintained in a specific pathogen–free animal facility according to institutional guidelines. Mice of the following genotypes and their intercrosses were bred in-house: C57BL/6J, *Gm38411*$^{iCre\text{-}hCD2}$ (11), *Rorc(t)*^{Cre} (57), *Vav*^{iCre}, R26^{tdTomato} (58), Rorc$_E$+7kb$^{\Delta/\Delta}$ (11), *Nr1d1/Nr1d2*$^{fl/fl}$ (38, 59), *Prdm16*$^{fl/fl}$ (60) and *Spi1*$^{fl/fl}$ (61). *Gm38411*$^{iCre\text{-}hCD2}$ mice were backcrossed to R26^{tdTomato} and to *Prdm16*$^{fl/fl}$. *Rorc(t)*^{Cre} mice were backcrossed to *Spi1*$^{fl/fl}$ mice. *Vav*^{iCre} mice were backcrossed to *Nr1d1/Nr1d2*$^{fl/fl}$ mice. The B6.SJL mice for BM chimera experiments as well as *Rag2*$^{-/-}$*γc*$^{-/-}$ mice were purchased from the Jackson Laboratory. Unless otherwise indicated, experiments used sex- and age-matched littermates of both sexes between 6 and 14 weeks of age.

Immune cell harvest

Immune cells were isolated as follows: BM progenitors were obtained from femurs, tibias, pelvic bones and humeri by mechanical disruption followed by single-cell filtration. Cells from spleen, sLN, cLN, and mLN were released by enzymatic digestion with collagenase D

(0.25 mg/ml) for 30 min at 37 °C. BM and spleen suspensions were subjected to red blood cell lysis using 1× RBC lysis buffer (BioLegend). All samples were passed through a 70-μm strainer prior to further processing. For small intestine lamina propria lymphocyte isolation, intestines were flushed with HBSS to remove luminal contents, then cut into pieces and washed for 20 min in HBSS containing 10% FCS and 5 mM EDTA. Tissue fragments were vortexed, washed again, and digested in RPMI containing collagenase IV (0.25 mg/ml) for 45 min with vigorous shaking at 37 °C. Remaining tissue debris was removed by filtration through a 100-μm mesh, and the flow-through was used for staining and intracellular cytokine assays. For cell sorting, samples were processed on a BD FACSAria II, with cells collected into PBS containing 0.5% BSA and 2.5 mM EDTA. Post-sort analysis confirmed ≥95% purity.

Cell culture

Total BM cells (1.5×10^6/ml) or sorted BM progenitors ($0.5–20\times10^3$) were cultured in RPMI (Gibco) supplemented with 10% fetal calf serum. To induce RORγt$^+$ DC development, cells were cultured in the presence of hFLT3L supernatant (10%) and complemented with mSCF supernatant (2%) and mIL-7 supernatant (5%). hFLT3L, mSCF, and mIL-7 were supplied as conditioned supernatants generated from cytokine-transfected mouse J558 myeloma cells. The myeloma-based expression system has been described previously by Traunecker et al. (62). Supernatants were harvested upon reaching cellular confluence, and the indicated percentages represent the final volume/volume (v/v) proportion of each cytokine-containing supernatant in the culture medium.

In vivo expansion of RORγt$^+$ DCs

To expand RORγt$^+$ DCs in vivo, *Gm38411*$^{\text{iCre-hCD2}}$ R26$^{\text{tdTomato}}$ mice were injected intraperitoneally with a 1:1:1 mixture of recombinant hFlt3L, mSCF, and mIL-7 supernatants (0.5ml/cytokine) on days 0, 1, 3, and 4. Mice were euthanized on day 7, and bone marrow, spleen, and mLNs were harvested to assess the expansion of *Rorc*$^+$ bone marrow cells, as well as RORγt$^+$ DCs and ILC3s.

BM chimeras

CD45.2$^+$ BM cells (5×10^6) were injected intravenously into sub lethally irradiated (= 550 cGy) CD45.1$^+$ congenic mice. For competitive transplantation experiments, 5×10^6 total CD45.1$^+$ BM cells were co-injected intravenously with 5×10^6 total BM cells from either CD45.2$^+$ C57BL/6 or CD45.2$^+$ Rorc$_{\text{E}}$+7kb$^{\Delta/\Delta}$ mice into sub lethally irradiated CD45.1/2$^+$ recipient mice. Recipient mice were analyzed 12 weeks post transfer. To assess the developmental potential of defined progenitor populations, $1–2\times10^4$ cells of sort-purified LMPP, IL-7R$^+$ LP, DN DCP and CDP from *Gm38411*$^{\text{iCre-hCD2}}$ R26$^{\text{tdTomato}}$ CD45.2$^+$ mice were injected intravenously into sublethally irradiated CD45.1$^+$ recipients. Recipient mice were analyzed 7 days post-transfer to assess the generation of RORγt$^+$ DCs and ILC3s. For experiments involving sort-purified *Rorc*$^+$ BM cell subsets, donor mice were first treated with cytokine supernatants to expand the progenitor compartment. Sorted cells were then injected intravenously into sublethally irradiated CD45.1$^+$ recipient mice and analyzed 3 days post-transfer.

ScRNAseq analysis

The Cell Ranger Software Suite (v8.0.1, 10x Genomics) was used for sample demultiplexing, barcode processing, and single-cell counting. The Cell Ranger "count" function was run using the mm10 reference genome, supplemented with tdTomato, iCre, and hCD2 gene sequences. Downstream analysis was performed in R using the Seurat package (v4.1.1). Demultiplexing was carried out with the HTODemux function. Quality control involved excluding cells with mitochondrial content >5–15%, fewer than 500–2,500 detected genes, or more than 7,500–9,500 detected genes per cell. Normalization was performed by log transformation with a scaling factor of 10,000. Dimensionality reduction and clustering were performed using RunUMAP, FindNeighbors, and FindClusters on the top 12–18 principal components, with a clustering resolution of 0.15–0.23. To allow cross-comparison of our dataset with three recently published datasets, datasets were merged and integrated in Seurat using canonical correlation analysis (CCA), followed by clustering and UMAP visualization.

10x Genomics ScRNAseq library preparation

Two scRNA-seq datasets were generated: one from in vitro–derived ILC3s and RORγt$^+$ DCs obtained from in vitro cultures derived from 15-day-old *Gm38411*$^{\text{iCre-hCD2}}$ R26$^{\text{tdTomato}}$ mice, and another from hCD2$^{+/-}$ tdTomato$^+$ cells isolated from BM, spleen, sLN, mLN, and cLN of both adult and 15-day-old *Gm38411*$^{\text{iCre-hCD2}}$ R26$^{\text{tdTomato}}$ mice. For the in vitro generated samples, BM from three 15 days old *Gm38411*$^{\text{iCre-hCD2}}$ R26$^{\text{tdTomato}}$ mice was cultured for 8 days under RORγt$^+$ DC–promoting conditions (FLT3L, SCF, and IL-7). Cells were then harvested and sorted as CD45$^+$ CD3$^-$ B220$^-$ Ly6C$^-$hCD2$^+$ tdTomato$^+$. Each sample was labeled with HT-10, HT-11, or HT-12 antibody hashtags, respectively. Enriched cells were pooled, resuspended in PBS containing 0.04% BSA at ~1,500 cells/μl, and loaded onto a 10x Genomics Chromium Single Cell Controller (super-loading protocol) at the McDonnell Genome Institute (MGI), Washington University in St. Louis. For the ex vivo scRNA-seq experiments, hCD2$^+$ tdTomato$^+$ and hCD2$^-$ tdTomato$^+$ cells were isolated from BM, spleen, sLN, mLN, and cLN of both 15-day-old pups and adult *Gm38411*$^{\text{iCre-hCD2}}$ R26$^{\text{tdTomato}}$ mice. For each condition, cells from four mice were pooled per organ. Pooled organs from 15-day-old pups were hashtagged as BM (HT-1), sLN (HT-4), mLN (HT-5), cLN (HT-6), and spleen (HT-7), while adult samples were hashtagged as BM (HT-8), sLN (HT-9), mLN (HT-10), cLN (HT-11), and spleen (HT-12). Two samples were prepared and loaded: one consisting of pooled hCD2$^+$ tdTomato$^+$ cells and the other of pooled hCD2$^-$ tdTomato$^+$ cells. Enriched cells were resuspended in PBS containing 0.04% BSA at ~1,500 cells/μl and super-loaded onto a 10x Genomics Chromium Single Cell Controller at the McDonnell Genome Institute (MGI), Washington University in St. Louis. The 10x Genomics Next GEM Single Cell 3′ Reagents Kit was used for library preparation on the 10x Genomics platform. Specifically, the Chromium Next GEM Single Cell 3′ Kit v4 (16 rxns), Chromium GEM-X Single Cell 3' Chip Kit v4, 4 chips, and Dual Index Kit TT Set A (96 rxns) were employed. In brief, up to 60,000 cells were partitioned into nanoliter Gel-bead-in-Emulsions (GEMs), each containing a reverse transcriptase reaction mix. Single-cell cDNA was assigned a unique 12-nucleotide barcode and unique molecular identifier (UMI). GEM cDNA then underwent 11 cycles of amplification and purification with SPRIselect beads. Gene expression (GEX) and hashtag-oligo (HTO) libraries were generated according

to the 10x Genomics Chromium Single Cell 3′ Reagent Kits User Guide, with PCR cycles adjusted based on cDNA concentration. Library concentrations were measured by qPCR using the KAPA Library Quantification Kit following the manufacturer's instructions (KAPA Biosystems/Roche). Normalized libraries were sequenced on a NovaSeqX plus S4 Flow Cell using the XP workflow and a 151×10×10×151 sequencing recipe according to the manufacturer protocol. A median sequencing depth of 50,000 reads per cell was targeted for GEX libraries and 5,000 reads per cell for HTO libraries.

Antibodies and flow cytometry

Cells were stained following established protocols using the antibodies listed in Antibody list of data file S4. To determine the frequency of tdTomato$^+$ cells within RORγt$^+$ cell subsets in hCD2^{Cre} R26^{tdTomato} mice, intracellular staining was performed using the FOXP3 Intracellular Staining Kit according to the manufacturer's instructions. For intracellular tdTomato stainings, cells were stained for 60 min with an anti-RFP antibody (1:200), followed by a 30-min incubation with a PE-conjugated anti-rabbit IgG secondary antibody (1:500). For PRDM16 detection, cells were incubated for 1 h with an anti-PRDM16 primary antibody (1:200), followed by a 30-min intracellular staining step with PE- or AF647-conjugated anti-rabbit secondary antibodies (1:500). Progenitors were gated as the following(11): LMPP = 7AAD$^-$ B220$^-$ Lin$^-$ CD117^{High} CD135$^+$; IL7R$^+$ LP = 7AAD$^-$ B220$^-$ Ly6C$^-$ Lin$^-$ CD117$^{Int/low}$ CD135$^+$ CD115$^-$ CD127$^+$; DN DCP = 7AAD$^-$ B220$^-$ Ly6C$^-$ Lin$^-$ CD117$^{Int/low}$ CD135$^+$ CD115$^-$ CD127$^-$; CDP = 7AAD$^-$ B220$^-$ Ly6C$^-$ Lin$^-$ CD117$^{Int/low}$ CD135$^+$ CD115$^+$ CD127$^-$. Mature DC subsets were gated as *Gm38411*-hCD2 or RORγt negative, thereby excluding RORγt$^+$ DC contamination. The lineage cocktail contains following antibodies: CD19, NK1.1, Ly6G, Ly6C, GR-1, CD105 and Ter119. Flow cytometric analysis was performed on a BD FACSymphony A3, and data were processed using FlowJo X software (Tree Star).

Quantification and statistical analysis:

Analysis of all data was done with an unpaired, two-tailed Student's t test and one-way ANOVA (Friedman test). (Prism, GraphPad Software Inc.). P values less than 0.05 were considered significant. *0.01 < P < 0.05; **0.001 < P < 0.01; ***P < 0.001; ****P < 0.0001.

Supplementary Material

Refer to Web version on PubMed Central for supplementary material.

Acknowledgments:

We thank Mitchell A. Lazar for providing the *Nr1d1/Nr1d2* floxed mice. We thank E. Lantelme for managing the Pathology and Immunology Flow Cytometry Core. We acknowledge the WUSM Genome Engineering and iPSC Center for gRNA validation, and M. White and the WUSM Transgenic/Knockout and Micro-Injection Core for mouse generation. We also thank the GTAC at the McDonnell Genome Institute at WUSM for scRNA-seq. GTAC is supported by the Washington University Institute of Clinical and Translational Sciences grant UL1TR002345 from NCATS of the NIH. Graphical illustrations were created with BioRender.com.

Funding:

This work was supported by National Institutes of Health grant RO1AI134035, RO1DK132327, RO1DK126969 and RO1DK124699 to M.Co. P.F.R. and S.W. were supported by SNF grants P2BSP3_191754/ P500PB_211033/ PS00-3_234543 and NIH grant T32DK077653, respectively.

Data, code, and materials availability:

ScRNA-seq data is deposited in the GEO database (GSE312414 and GSE312479). The scATAC–seq data of ILC3s derived from *Nr1d1/Nr1d2*$^{fl/fl}$ and *Vav*^{iCre} *Nr1d1/Nr1d2*$^{fl/fl}$ mice were published in Bhattarai et al. (38) and are deposited in the GEO database (GSE267792). No custom code was generated in this study. Tabulated data underlying the figures is provided in data file S5. All other data needed to support the conclusions of the paper are present in the paper or the Supplementary Materials. Reagents described in this manuscript and previously generated in Prof. M. Colonna's laboratory are available from Prof. M. Colonna under a Material Transfer Agreement (MTA) from Washington University School of Medicine in St. Louis. All other materials are commercially available, as described in the Materials and Methods and in Data File S4.

References

1. Esterhazy D et al. , Compartmentalized gut lymph node drainage dictates adaptive immune responses. Nature 569, 126–130 (2019). [PubMed: 30988509]
2. Campos Canesso MC et al. , Identification of antigen-presenting cell-T cell interactions driving immune responses to food. Science 387, eado5088 (2025). [PubMed: 39700315]
3. Ramanan D et al. , Regulatory T cells in the face of the intestinal microbiota. Nat Rev Immunol 23, 749–762 (2023). [PubMed: 37316560]
4. Brown CC et al. , Transcriptional Basis of Mouse and Human Dendritic Cell Heterogeneity. Cell 179, 846–863 e824 (2019). [PubMed: 31668803]
5. Akagbosu B et al. , Novel antigen-presenting cell imparts T(reg)-dependent tolerance to gut microbiota. Nature 610, 752–760 (2022). [PubMed: 36070798]
6. Kedmi R et al. , A RORgammat(+) cell instructs gut microbiota-specific T(reg) cell differentiation. Nature 610, 737–743 (2022). [PubMed: 36071167]
7. Lyu M et al. , ILC3s select microbiota-specific regulatory T cells to establish tolerance in the gut. Nature 610, 744–751 (2022). [PubMed: 36071169]
8. Fu L et al. , PRDM16-dependent antigen-presenting cells induce tolerance to gut antigens. Nature 642, 756–765 (2025). [PubMed: 40228524]
9. Cabric V et al. , A wave of Thetis cells imparts tolerance to food antigens early in life. Science 389, 268–274 (2025). [PubMed: 40373113]
10. Ulezko Antonova A et al. , A distinct human cell type expressing MHCII and RORgammat with dual characteristics of dendritic cells and type 3 innate lymphoid cells. Proc Natl Acad Sci U S A 120, e2318710120 (2023).
11. Rodrigues PF et al. , Rorgammat-positive dendritic cells are required for the induction of peripheral regulatory T cells in response to oral antigens. Cell 188, 2720–2737 e2722 (2025). [PubMed: 40185101]
12. Narasimhan H et al. , RORgammat-expressing dendritic cells are functionally versatile and evolutionarily conserved antigen-presenting cells. Proc Natl Acad Sci U S A 122, e2417308122 (2025).
13. Wang J et al. , Single-cell multiomics defines tolerogenic extrathymic Aire-expressing populations with unique homology to thymic epithelium. Sci Immunol 6, eabl5053 (2021). [PubMed: 34767455]

14. Sun IH et al. , RORgammat eTACs mediate oral tolerance and Treg induction. J Exp Med 222, (2025).
15. Ogawa C et al. , Runx/Cbfbeta regulates the development of tolerogenic Thetis cells. bioRxiv, (2025).
16. Eberl G et al. , An essential function for the nuclear receptor RORgamma(t) in the generation of fetal lymphoid tissue inducer cells. Nat Immunol 5, 64–73 (2004). [PubMed: 14691482]
17. Ivanov II et al. , The orphan nuclear receptor RORgammat directs the differentiation program of proinflammatory IL-17+ T helper cells. Cell 126, 1121–1133 (2006). [PubMed: 16990136]
18. Eberl G, RORgammat, a multitask nuclear receptor at mucosal surfaces. Mucosal Immunol 10, 27–34 (2017). [PubMed: 27706126]
19. Fogg DK et al. , A clonogenic bone marrow progenitor specific for macrophages and dendritic cells. Science 311, 83–87 (2006). [PubMed: 16322423]
20. Liu Z et al. , Dendritic cell type 3 arises from Ly6C(+) monocyte-dendritic cell progenitors. Immunity, (2023).
21. Naik SH et al. , Development of plasmacytoid and conventional dendritic cell subtypes from single precursor cells derived in vitro and in vivo. Nat Immunol 8, 1217–1226 (2007). [PubMed: 17922015]
22. Onai N et al. , Identification of clonogenic common Flt3+M-CSFR+ plasmacytoid and conventional dendritic cell progenitors in mouse bone marrow. Nat Immunol 8, 1207–1216 (2007). [PubMed: 17922016]
23. Cabeza-Cabrerizo M, Cardoso A, Minutti CM, Pereira da Costa M, Reis e Sousa C, Dendritic Cells Revisited. Annu Rev Immunol 39, 131–166 (2021). [PubMed: 33481643]
24. Sathe P, Vremec D, Wu L, Corcoran L, Shortman K, Convergent differentiation: myeloid and lymphoid pathways to murine plasmacytoid dendritic cells. Blood 121, 11–19 (2013). [PubMed: 23053574]
25. Rodrigues PF et al. , Distinct progenitor lineages contribute to the heterogeneity of plasmacytoid dendritic cells. Nat Immunol 19, 711–722 (2018). [PubMed: 29925996]
26. Dress RJ et al. , Plasmacytoid dendritic cells develop from Ly6D(+) lymphoid progenitors distinct from the myeloid lineage. Nat Immunol 20, 852–864 (2019). [PubMed: 31213723]
27. Harly C et al. , The transcription factor TCF-1 enforces commitment to the innate lymphoid cell lineage. Nat Immunol 20, 1150–1160 (2019). [PubMed: 31358996]
28. Rodrigues PF et al. , Progenitors of distinct lineages shape the diversity of mature type 2 conventional dendritic cells. Immunity 57, 1567–1585 e1565 (2024). [PubMed: 38821051]
29. Kanayama M et al. , Diverse developmental pathways of lymphoid conventional dendritic cells with distinct tissue distribution and function. Sci Adv 11, eadt4909 (2025). [PubMed: 40479074]
30. Minutti CM et al. , Distinct ontogenetic lineages dictate cDC2 heterogeneity. Nat Immunol 25, 448–461 (2024). [PubMed: 38351322]
31. Zhu Y et al. , Transcription factors TCF4 and KLF4 respectively control the development of the DC2A and DC2B lineages. Nat Immunol 26, 1275–1286 (2025). [PubMed: 40702338]
32. Papaioannou NE et al. , Environmental signals rather than layered ontogeny imprint the function of type 2 conventional dendritic cells in young and adult mice. Nat Commun 12, 464 (2021). [PubMed: 33469015]
33. Rodrigues PF et al. , pDC-like cells are pre-DC2 and require KLF4 to control homeostatic CD4 T cells. Sci Immunol 8, eadd4132 (2023). [PubMed: 36827419]
34. de Boer J et al. , Transgenic mice with hematopoietic and lymphoid specific expression of Cre. Eur J Immunol 33, 314–325 (2003). [PubMed: 12548562]
35. Wang Y et al. , The intestinal microbiota regulates body composition through NFIL3 and the circadian clock. Science 357, 912–916 (2017). [PubMed: 28860383]
36. Wang Q et al. , Circadian rhythm-dependent and circadian rhythm-independent impacts of the molecular clock on type 3 innate lymphoid cells. Sci Immunol 4, (2019).
37. Teng F et al. , A circadian clock is essential for homeostasis of group 3 innate lymphoid cells in the gut. Sci Immunol 4, (2019).

38. Bhattarai B et al. , Circadian circuits control plasticity of group 3 innate lymphoid cells by sustaining epigenetic configuration of RORgammat. Nat Immunol 26, 1527–1539 (2025). [PubMed: 40804530]
39. Aguilo F et al. , Prdm16 is a physiologic regulator of hematopoietic stem cells. Blood 117, 5057–5066 (2011). [PubMed: 21343612]
40. Wang Q et al. , Post-translational control of beige fat biogenesis by PRDM16 stabilization. Nature 609, 151–158 (2022). [PubMed: 35978186]
41. Gudmundsson KO et al. , Prdm16 is a critical regulator of adult long-term hematopoietic stem cell quiescence. Proc Natl Acad Sci U S A 117, 31945–31953 (2020). [PubMed: 33268499]
42. Stine RR et al. , PRDM16 Maintains Homeostasis of the Intestinal Epithelium by Controlling Region-Specific Metabolism. Cell Stem Cell 25, 830–845 e838 (2019). [PubMed: 31564549]
43. Nah J, Lee Y, Seong RH, PRDM16 regulates gammadeltaT17 cell differentiation via controlling type 17 program and lipid-dependent cell fitness. Front Immunol 14, 1332386 (2023). [PubMed: 38239368]
44. Seale P et al. , PRDM16 controls a brown fat/skeletal muscle switch. Nature 454, 961–967 (2008). [PubMed: 18719582]
45. Mak KS, Funnell AP, Pearson RC, Crossley M, PU.1 and Haematopoietic Cell Fate: Dosage Matters. Int J Cell Biol 2011, 808524 (2011). [PubMed: 21845190]
46. Rothenberg EV, Hosokawa H, Ungerback J, Mechanisms of Action of Hematopoietic Transcription Factor PU.1 in Initiation of T-Cell Development. Front Immunol 10, 228 (2019). [PubMed: 30842770]
47. Pang SHM et al. , PU.1 Is Required for the Developmental Progression of Multipotent Progenitors to Common Lymphoid Progenitors. Front Immunol 9, 1264 (2018). [PubMed: 29942304]
48. Nutt SL, Chopin M, Transcriptional Networks Driving Dendritic Cell Differentiation and Function. Immunity 52, 942–956 (2020). [PubMed: 32553180]
49. Chopin M et al. , Transcription Factor PU.1 Promotes Conventional Dendritic Cell Identity and Function via Induction of Transcriptional Regulator DC-SCRIPT. Immunity 50, 77–90 e75 (2019). [PubMed: 30611612]
50. Carotta S et al. , The transcription factor PU.1 controls dendritic cell development and Flt3 cytokine receptor expression in a dose-dependent manner. Immunity 32, 628–641 (2010). [PubMed: 20510871]
51. Salvermoser J et al. , Clec9a-Mediated Ablation of Conventional Dendritic Cells Suggests a Lymphoid Path to Generating Dendritic Cells In Vivo. Front Immunol 9, 699 (2018). [PubMed: 29713321]
52. Wang C et al. , Role of circadian transcription factor REV-ERB in cardiovascular diseases: a review. Front Cardiovasc Med 12, 1516279 (2025). [PubMed: 40255337]
53. Akiyama T, Shinzawa M, Akiyama N, TNF receptor family signaling in the development and functions of medullary thymic epithelial cells. Front Immunol 3, 278 (2012). [PubMed: 22969770]
54. Rossi SW et al. , RANK signals from CD4(+)3(−) inducer cells regulate development of Aire-expressing epithelial cells in the thymic medulla. J Exp Med 204, 1267–1272 (2007). [PubMed: 17502664]
55. Haljasorg U et al. , A highly conserved NF-kappaB-responsive enhancer is critical for thymic expression of Aire in mice. Eur J Immunol 45, 3246–3256 (2015). [PubMed: 26364592]
56. LaFlam TN et al. , Identification of a novel cis-regulatory element essential for immune tolerance. J Exp Med 212, 1993–2002 (2015). [PubMed: 26527800]
57. Eberl G, Littman DR, Thymic origin of intestinal alphabeta T cells revealed by fate mapping of RORgammat+ cells. Science 305, 248–251 (2004). [PubMed: 15247480]
58. Madisen L et al. , A robust and high-throughput Cre reporting and characterization system for the whole mouse brain. Nat Neurosci 13, 133–140 (2010). [PubMed: 20023653]
59. Dierickx P et al. , SR9009 has REV-ERB-independent effects on cell proliferation and metabolism. Proc Natl Acad Sci U S A 116, 12147–12152 (2019). [PubMed: 31127047]
60. Corrigan DJ et al. , PRDM16 isoforms differentially regulate normal and leukemic hematopoiesis and inflammatory gene signature. J Clin Invest 128, 3250–3264 (2018). [PubMed: 29878897]

61. Iwasaki H et al. , Distinctive and indispensable roles of PU.1 in maintenance of hematopoietic stem cells and their differentiation. Blood 106, 1590–1600 (2005). [PubMed: 15914556]

62. Traunecker A, Oliveri F, Karjalainen K, Myeloma based expression system for production of large mammalian proteins. Trends Biotechnol 9, 109–113 (1991). [PubMed: 1367388]

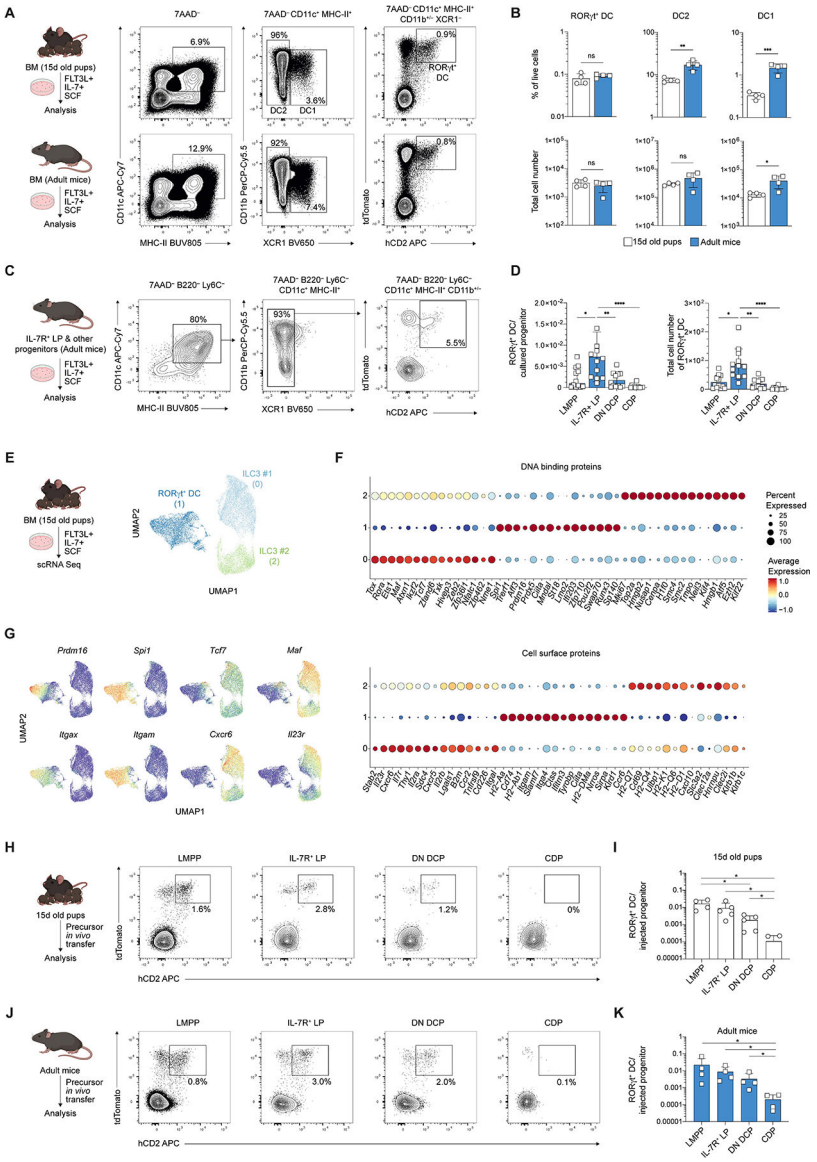

Fig. 1. RORγt$^+$ DCs originate from lymphoid progenitors independent of age.

(A–B) Total BM cells from 15-day-old pups (top) or adults (bottom) of *Gm38411*$^{iCre\text{-}hCD2}$ R26^{tdTomato} mice were cultured for 8 days with FLT3L, SCF, and IL-7 and analyzed for RORγt$^+$ DCs. (A) Representative gating strategy for indicated DC subsets (n=4 mice). (B) Frequencies (top) and total cell numbers (bottom) of DC subsets (mean ± SD, n=4 mice). (C–D) Sorted BM progenitors from adult mice were cultured for 4 days with FLT3L, SCF, and IL-7. (C) Representative gating of IL-7R$^+$ LP–derived RORγt$^+$ DCs (n=11 mice). (D) Ratios of RORγt$^+$ DCs per cultured progenitor (left) and total RORγt$^+$ DC numbers (right) (mean ± SD, n=11 mice). (E) scRNA-seq UMAP projection of B220$^-$ CD3$^-$Ly6C$^-$ tdTomato$^+$hCD2$^+$ cells (ILC3s and RORγt$^+$ DCs) from BM cultures of 15-day-old mice (n=3 mice). (F) Dot plots of differentially expressed DNA-binding proteins (top) and cell surface proteins (bottom) across clusters. (G) Featureplot visualization of selected marker genes. (H–K) Sorted progenitors from 15-day-old pups (H–I) or adults

(J–K) were transferred into sublethally irradiated CD45.1 hosts, and splenic RORγt$^+$ DCs were analyzed 7 days later. (H, J) Representative gating of in vivo–differentiated CD45.1$^-$ CD45.2$^+$ B220$^-$ CD3$^-$ CD11c$^+$ MHC-II$^+$ XCR1$^-$ CD11b$^{+/-}$ tdTomato$^+$ hCD2$^+$ RORγt$^+$ DCs (n=4 mice). (I, K) Ratios of RORγt$^+$ DCs per transferred progenitor (mean ± SD, n=4 mice). Statistical significance was determined using unpaired two-tailed t-test (Fig .1, B, I and K) or one-way ANOVA (Friedman test) (Fig.1D). *0.01 < P < 0.05; **0.001 < P < 0.01; ***P < 0.001; ****P < 0.0001.; ns, not significant.

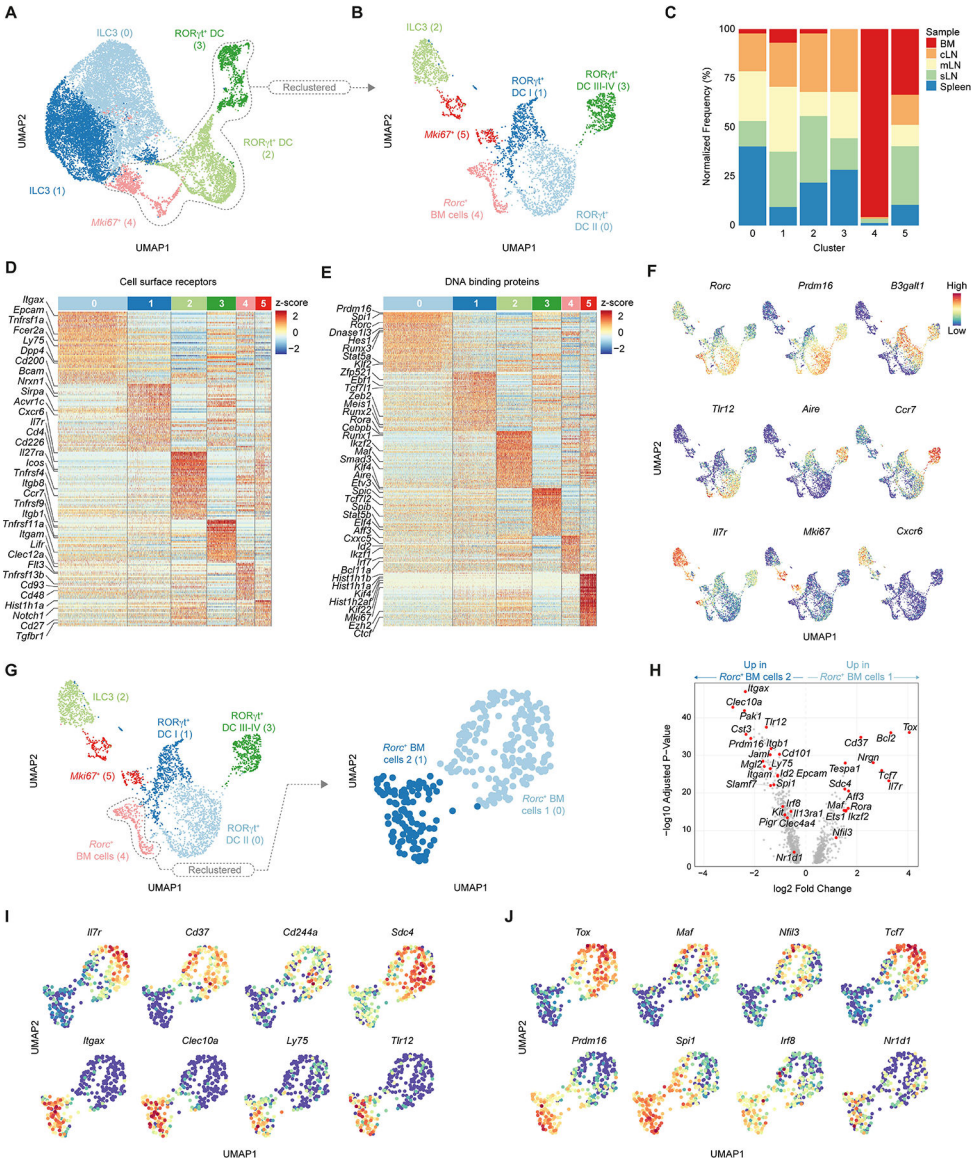

Fig. 2. RORγt$^+$ DC subsets are distributed across lymphoid tissues.

(A) scRNA-seq UMAP projection of B220$^-$ CD3$^-$ Ly6C$^-$ tdTomato$^+$ hCD2$^+$ cells from BM, spleen, cLN, mLN, and sLN of 15-day-old and adult mice (n=4 mice for each organ at each age). (B) UMAP projection of reclustered cells from clusters 2, 3, and 4 in (A). (C) Normalized tissue distribution of clusters shown in (B). (D–E) Heatmaps of differentially expressed cell surface (D) and DNA-binding (E) proteins across clusters. (F) Feature plots of selected marker genes. (G) UMAP projection of reclustered *Rorc*$^+$ BM cells. (H) Volcano plot of differentially expressed genes between *Rorc*$^+$ BM cells 1 (Cluster 0) and *Rorc*$^+$ BM cells 2 (Cluster 1). (I–J) Feature plots of selected cell surface receptors (I) and transcription factors (J).

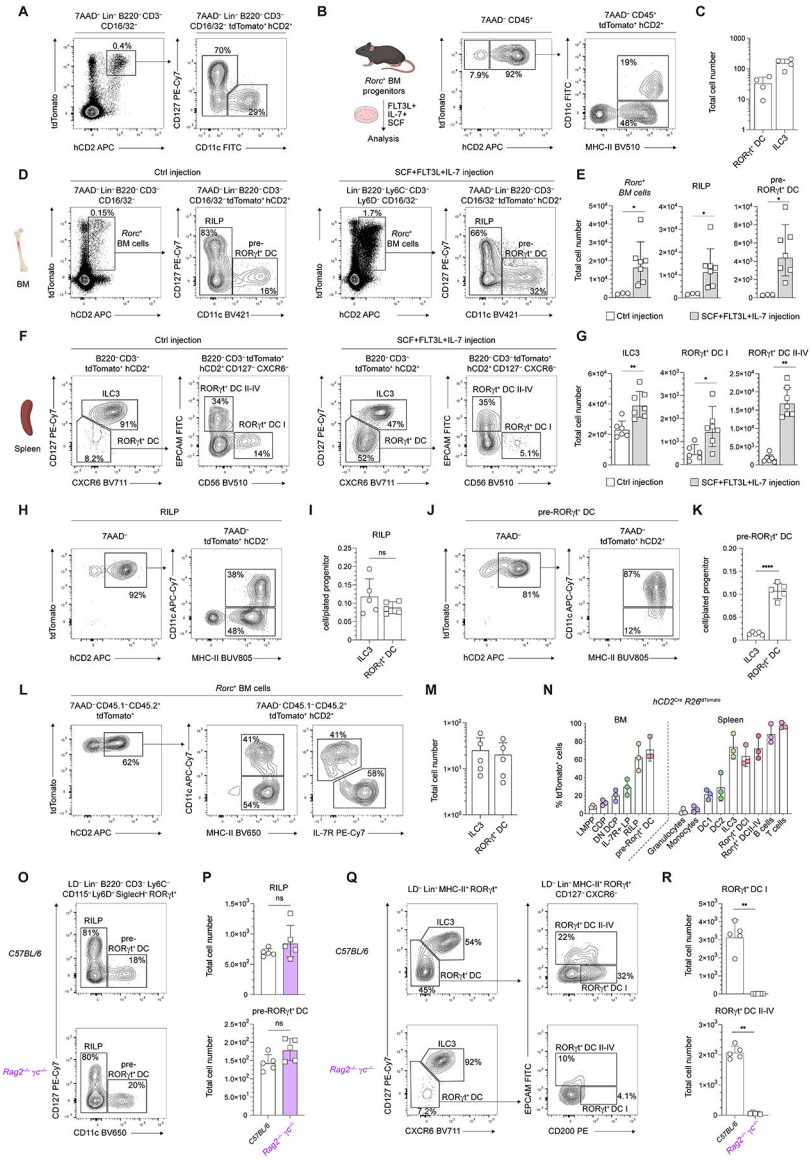

Fig. 3. RORγt$^+$ DCs arise from lymphoid-derived *Rorc*$^+$ BM progenitors.

(A) Gating of CD11c$^+$ pre-RORγt$^+$ DCs and CD127$^+$ RILP within Lin$^-$ CD3$^-$CD16/32$^-$ B220$^-$tdTomato$^+$hCD2$^+$ *Rorc*$^+$ BM cells from adult *Gm38411*$^{iCre\text{-}hCD2}$R26^{tdTomato} mice (n=4 mice). (B–C) Sorted *Rorc*$^+$ BM cells from adult mice were cultured for 3 days with FLT3L+SCF+IL-7 (n=4 mice). (B) Gating of hCD2$^+$tdTomato$^+$CD11c$^+$MHC-II$^+$ RORγt$^+$ DCs and hCD2$^+$tdTomato$^+$CD11c$^-$MHC-II$^+$ ILC3s derived from *Rorc*$^+$ BM cells. (C) Total numbers of RORγt$^+$ DCs and ILC3s after 3 days of culture (mean±SD, n=4 mice). (D-G) Adult *Gm38411*$^{iCre\text{-}hCD2}$R26^{tdTomato} mice were treated with FLT3L+SCF+IL-7. (D) Gating of *Rorc*$^+$ BM cells, pre-RORγt$^+$ DC and RILP in adult BM from ctrl and cytokine-treated mice. (E) Total progenitor numbers after indicated treatments (mean±SD, n=3–7 mice). (F) Gating of splenic ILC3s and RORγt$^+$ DCs in ctrl and cytokine-treated adult mice. (G) Total splenic ILC3s and RORγt$^+$ DCs after indicated treatments (mean±SD, n=6–7 mice).

(H-K) RILP or pre-RORγt^{+} DCs were sorted from cytokine-treated adult *Gm38411*$^{iCre\text{-}hCD2}$R26^{tdTomato} mice and cultured. ILC3 and RORγt^{+} DC output was assessed after 3 days. Gating of ILC3s and RORγt^{+} DCs derived from RILP (H) and pre-RORγt^{+} DCs (J). Output of ILC3s and RORγt^{+} DCs derived from RILP (I) and pre-RORγt^{+} DCs (K). (L-M) Expanded *Rorc*$^{+}$ BM cells from *Gm38411*$^{iCre\text{-}hCD2}$R26^{tdTomato} mice were sorted and adoptively transferred into sub-lethally irradiated CD45.1 hosts. Splenic reconstitution was analyzed 3 days after. (L) Gating of splenic donor derived CD11c^{-}MHC-II^{+}IL-7R^{+} ILC3s and CD11c^{+}MHC-II^{+}IL-7R^{-} RORγt^{+} DCs. (M) Total numbers of donor derived splenic ILC3 and RORγt^{+} DC subsets (mean±SD, n=5 mice). (N) tdTomato frequencies in BM and splenic immune cell subsets of adult *hCD2*^{Cre}R26^{tdTomato} mice (n=3 mice). (O) Gating of RILP and pre-RORγt^{+} DCs in C57BL/6 and *Rag2*$^{-/-}$γc$^{-/-}$ mice. (P) Total numbers of indicated progenitors in C57BL/6 and Rag2$^{-/-}$γc$^{-/-}$ mice (mean±SD, n=5 mice). (Q) Gating of splenic ILC3s and RORγt^{+} DCs in C57BL/6 and Rag2$^{-/-}$γc$^{-/-}$ mice. (R) Total RORγt^{+} DCs in C57BL/6 and Rag2$^{-/-}$γc$^{-/-}$ mice (mean±SD, n=5 mice). Statistical significance was determined by unpaired two-tailed t-test. *0.01<P<0.05; **0.001<P<0.01; ****P<0.0001; ns, not significant.

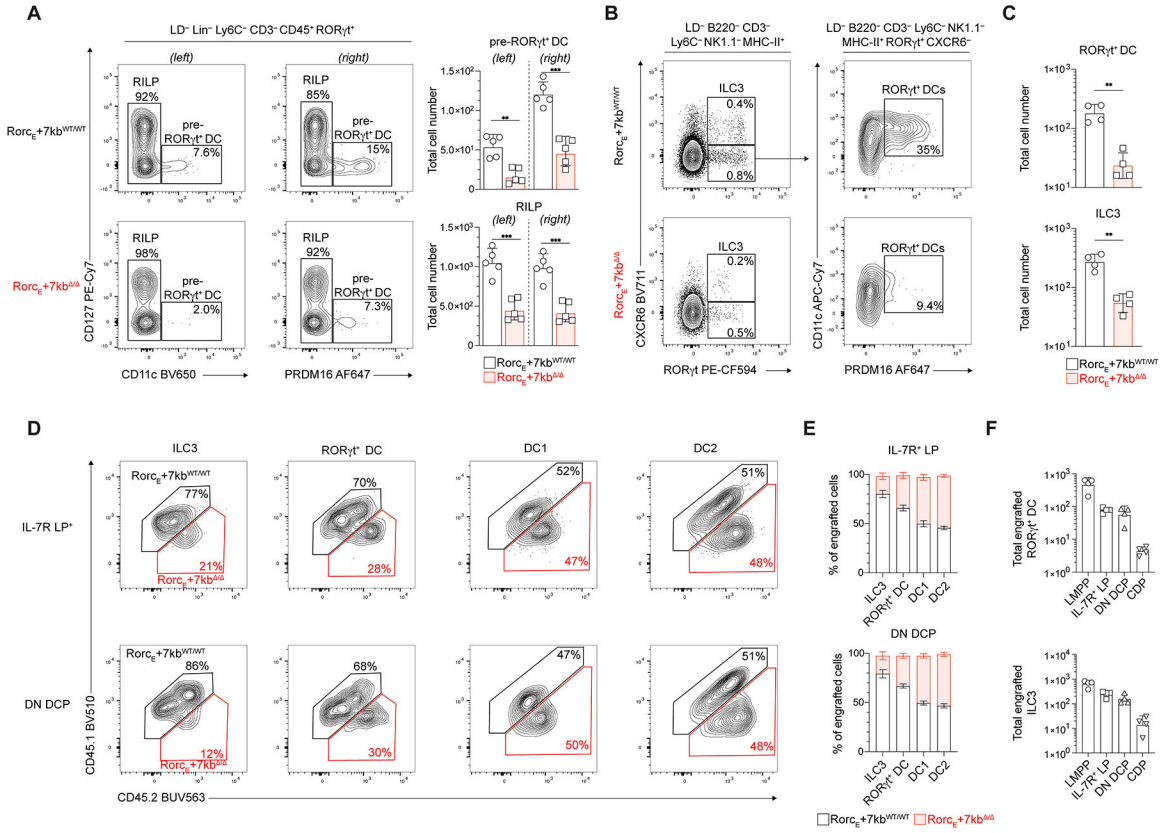

Fig. 4. The *Rorc* +7kb enhancer is essential for RORγt$^+$ DC development.

(A) Frequencies and total numbers of pre-RORγt$^+$ DCs and RILP in the bone marrow of adult Rorc$_E$+7kb$^{WT/WT}$ and Rorc$_E$+7kb$^{Δ/Δ}$ mice (n=5 mice). Representative flow cytometry plots from Rorc$_E$+7kb$^{WT/WT}$ (top) and Rorc$_E$+7kb$^{Δ/Δ}$ (bottom) bone marrow show gating of pre-RORγt$^+$ DCs using CD11c (left) or intracellular PRDM16 (right). Quantification of total pre-RORγt$^+$ DCs (top right) and RILP (bottom right) is shown (mean ± SD). (B–C) Total BM cells from adult Rorc$_E$+7kb$^{WT/WT}$ and Rorc$_E$+7kb$^{Δ/Δ}$ mice were cultured for 8 days with FLT3L, SCF, and IL-7. (B) Representative gating of ILC3s and RORγt$^+$ DCs (n=4 mice). (C) Total cell numbers of RORγt$^+$ DCs (top) and ILC3s (bottom) (mean ± SD, n=4 mice). (D–F) Competitive chimeras were generated by transferring CD45.1/2$^+$ Rorc$_E$+7kb$^{WT/WT}$ (black) and CD45.2$^+$ Rorc$_E$+7kb$^{Δ/Δ}$ (red) sorted progenitors into sub-lethally irradiated CD45.1$^+$ congenic hosts and analyzed 7 days later (n=4 mice). (D) Representative flow cytometry plots showing engraftment ratios of indicated immune subsets in spleen after reconstitution with IL-7R$^+$ LP (top) and DN DCP (bottom). (E) Frequencies of engrafted subsets (mean ± SD, n=4 mice). (F) Total numbers of engrafted splenic RORγt$^+$ DCs and ILC3s derived from indicated progenitors (mean ± SD, n=4 mice). Statistical significance was determined by unpaired two-tailed t-test. **0.001 < P < 0.01; ***P < 0.001; ns, not significant.

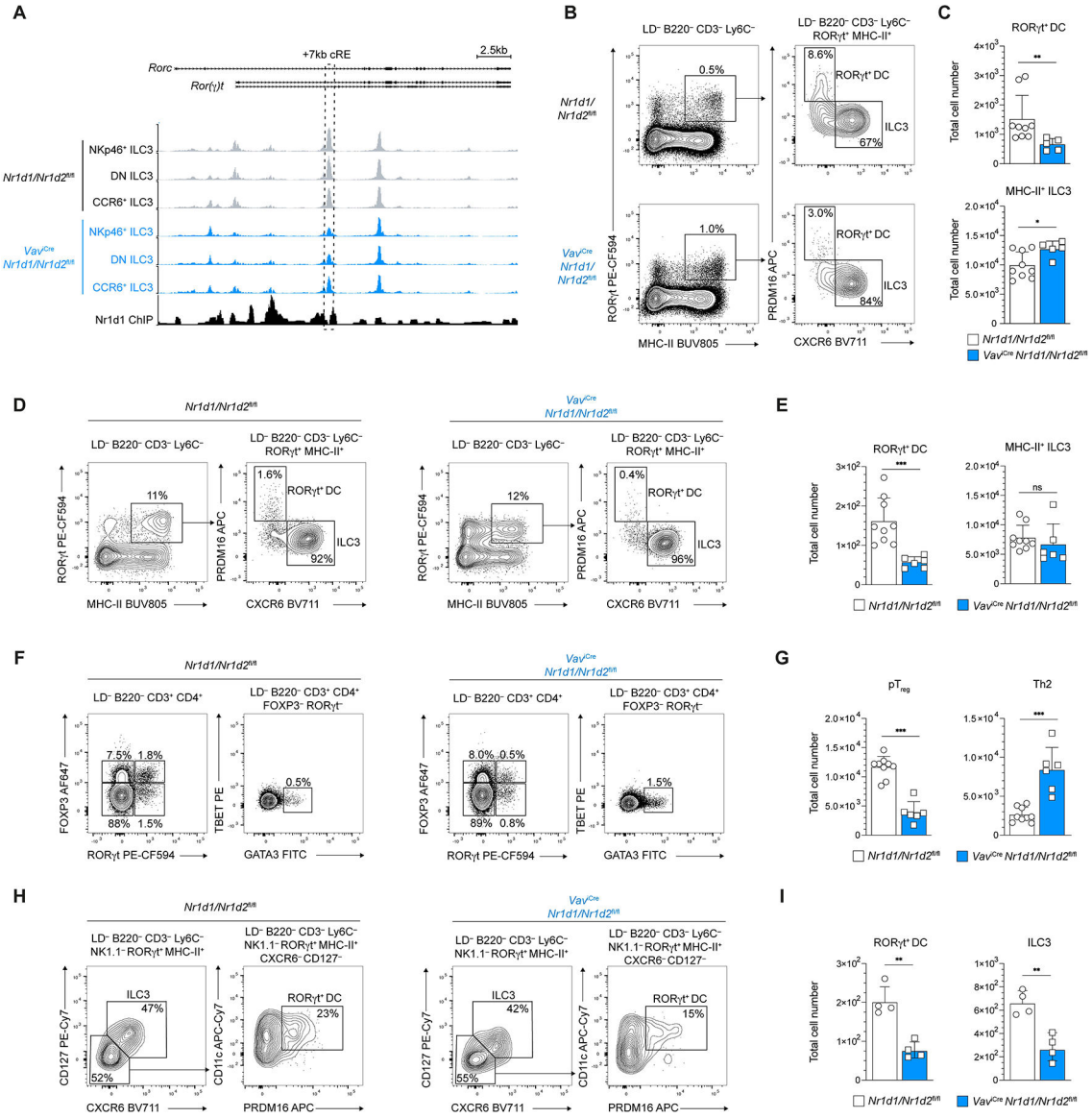

Fig. 5. REV-ERBα and REV-ERBβ promote RORγt$^+$ DC development through regulation of *Rorc* +7kbE.

(A) Pseudobulk ATAC–seq peaks at the *Rorc* locus in *Nr1d1/Nr1d2*$^{fl/fl}$ and *Vav*^{iCre} *Nr1d1/Nr1d2*$^{fl/fl}$ NKp46$^+$, DN, and CCR6$^+$ ILC3s, shown alongside REV-ERBα ChIP–seq. (B–C) RORγt$^+$ DC and ILC3 frequencies in spleens of adult *Nr1d1/Nr1d2*$^{fl/fl}$ and *Vav*^{iCre} *Nr1d1/Nr1d2*$^{fl/fl}$ mice (n=5–9 mice). (B) Representative gating of CXCR6$^+$ ILC3s and PRDM16$^+$ RORγt$^+$ DCs in control (top) and *Vav*^{iCre} (bottom) mice (n=5–9 mice). (C) Total cell numbers of RORγt$^+$ DCs (top) and ILC3s (bottom) (mean ± SD, n=5–9 mice). (D–E) RORγt$^+$ DC and ILC3 frequencies in mLN from adult *Nr1d1/Nr1d2*$^{fl/fl}$ and *Vav*^{iCre} *Nr1d1/Nr1d2*$^{fl/fl}$ mice (n=6–9 mice). (D) Representative gating in control (top) and *Vav*^{iCre} *Nr1d1/Nr1d2*$^{fl/fl}$ (bottom) mice (n=6–9 mice). (E) Total cell numbers of RORγt$^+$ DCs (top) and ILC3s (bottom) (mean ± SD, n=6–9 mice). (F–G) CD4$^+$ T cell subsets in mLN from adult *Nr1d1/Nr1d2*$^{fl/fl}$ and *Vav*^{iCre} *Nr1d1/Nr1d2*$^{fl/fl}$ mice (n=6–9 mice). (F) Representative gating of CD4$^+$ T cell subsets (n=6–9 mice). (G) Total numbers of indicated subsets (mean

± SD, n=6–9 mice). (H-I) Total BM cells from adult *Nr1d1/Nr1d2*$^{fl/fl}$ and *Vav*^{iCre} *Nr1d1/Nr1d2*$^{fl/fl}$ mice were cultured for 8 days with FLT3L, SCF, and IL-7 (n=4 mice). (H) Representative gating of CXCR6^{+} CD127^{+} ILC3s and CD11c^{+} PRDM16^{+} RORγt^{+} DCs (n=4 mice). (I) Total cell numbers of RORγt^{+} DCs and ILC3s (mean ± SD, n=4 mice). Statistical significance was determined by unpaired two-tailed t-test. *0.01 < P < 0.05; **0.001 < P < 0.01; ***P < 0.001; ns, not significant.

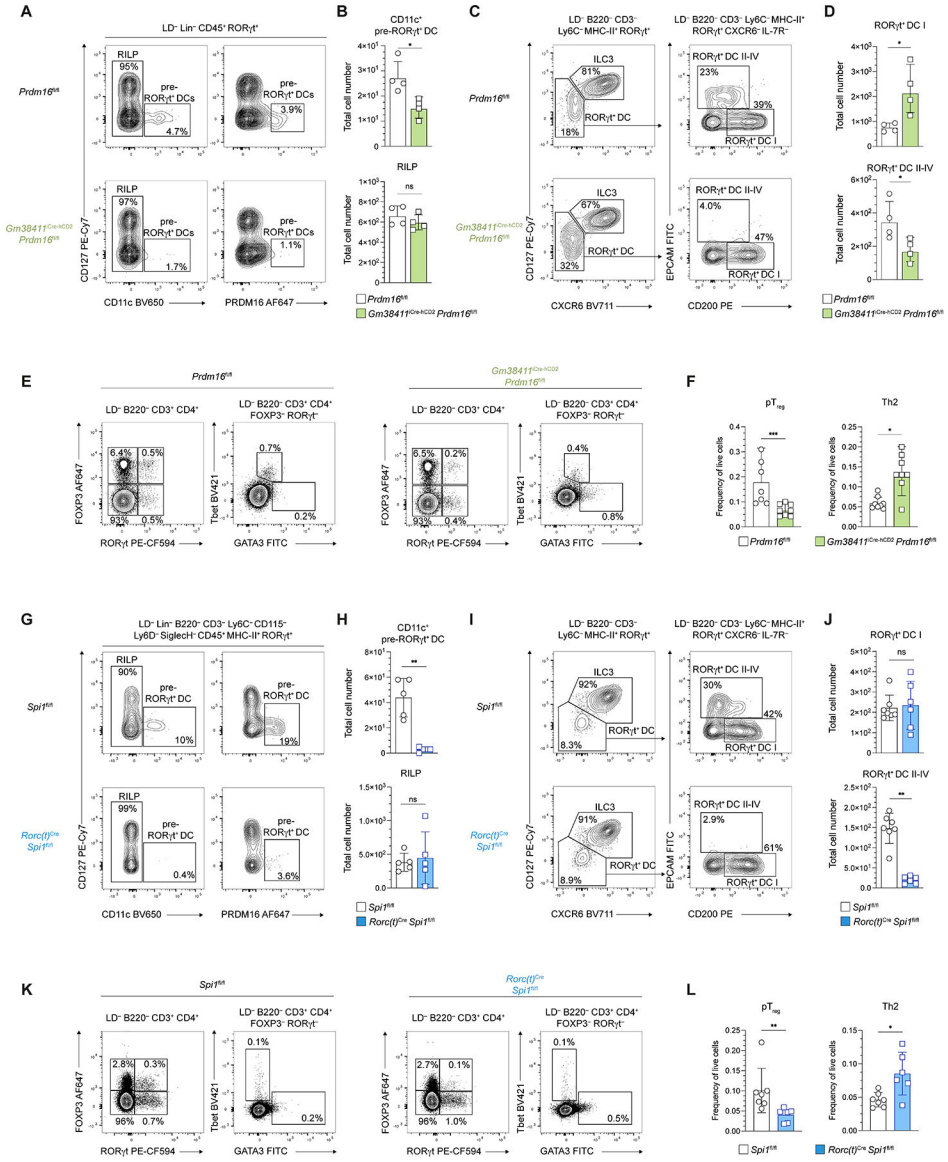

Fig. 6. PRDM16 and PU.1 are essential for the development of pre-RORγt^{+} DCs.

(A-B) Pre-RORγt^{+} DCs and RILP frequencies in BM of adult *Prdm16*$^{fl/fl}$ and *Gm38411*$^{iCre\text{-}hCD2}$ *Prdm16*$^{fl/fl}$ mice (n=4 mice). (A) Representative gating of RILP and CD11c^{+} (left) or PRDM16^{+} (right) RORγt^{+} DCs in control (top) and *Gm38411*$^{iCre\text{-}hCD2}$ *Prdm16*$^{fl/fl}$ (bottom) mice (n=4 mice). (B) Total cell numbers of CD11c^{+} pre-RORγt^{+} DCs (top) and RILP (bottom) (mean ± SD, n=4 mice). (C and D) RORγt^{+} DC and ILC3 frequencies in mLN from adult *Prdm16*$^{fl/fl}$ and *Gm38411*$^{iCre\text{-}hCD2}$ *Prdm16*$^{fl/fl}$ mice (n=4 mice). (C) Representative gating in control (top) and *Gm38411*$^{iCre\text{-}hCD2}$ *Prdm16*$^{fl/fl}$ (bottom) mice (n=4 mice). (D) Total cell numbers of RORγt^{+} DC I (top) and RORγt^{+} DC II-IV (bottom) (mean ± SD, n=4 mice). (E-F) CD4^{+} T cell subsets in mLN from adult *Prdm16*$^{fl/fl}$ and *Gm38411*$^{iCre\text{-}hCD2}$ *Prdm16*$^{fl/fl}$ mice (n=4 mice). (E) Representative gating of CD4^{+} T cell subsets. (F) Frequencies of indicated subsets (mean ± SD, n=4 mice). (G-H) Pre-RORγt^{+} DC and RILP frequencies in BM of adult *Spi1*$^{fl/fl}$ and *Rorc(t)*^{Cre} *Spi1*$^{fl/fl}$ mice (n=5 mice).

(G) Representative gating of RILP and CD11c^{+} (left) or PRDM16^{+} (right) pre-RORγt^{+} DCs in control (top) and *Rorc(t)*^{Cre} *Spi1*$^{fl/fl}$ (bottom) mice (n=5 mice). (H) Total cell numbers of CD11c^{+} pre-RORγt^{+} DCs (top) and RILP (bottom) (mean ± SD, n=5 mice). (I-J) RORγt^{+} DC and ILC3 frequencies in mLN from adult *Spi1*$^{fl/fl}$ and *Rorc(t)*^{Cre} *Spi1*$^{fl/fl}$ mice (n=6–7 mice). (I) Representative gating in control (top) and *Rorc(t)*^{Cre} *Spi1*$^{fl/fl}$ (bottom) mice (n=6–7 mice). (J) Total cell numbers of RORγt^{+} DC I (top) and RORγt^{+} DC II-IV (bottom) (mean ± SD, n=6–7 mice). (K-L) CD4^{+} T cell subsets in mLN from adult *Rorc(t)*^{Cre} *Spi1*$^{fl/fl}$ mice (n=6–7 mice). (K) Representative gating of CD4^{+} T cell subsets (n=6–7 mice). (L) Total numbers of indicated subsets (mean ± SD, n=6–7 mice). Statistical significance was determined by unpaired two-tailed t-test. *0.01 < P < 0.05; **0.001 < P < 0.01; ***P < 0.001; ns, not significant.